Journal Pre-proofs

Probing the stability of perovskite solar cell under working condition through an ultra-thin silver electrode: beyond the halide ion diffusion and metal diffusion

Hao Li, Zheng Yan, Min Li, Xiaoyan Wen, Shuo Deng, Sisi Liu, Wallace C. H. Choy, Lijie Li, Ming-Yu Li, Haifei Lu

PII: S1385-8947(23)00136-5
DOI: https://doi.org/10.1016/j.cej.2023.141405
Reference: CEJ 141405

To appear in: *Chemical Engineering Journal*

Received Date: 6 October 2022
Revised Date: 17 December 2022
Accepted Date: 9 January 2023

Please cite this article as: H. Li, Z. Yan, M. Li, X. Wen, S. Deng, S. Liu, W. C. H. Choy, L. Li, M-Y. Li, H. Lu, Probing the stability of perovskite solar cell under working condition through an ultra-thin silver electrode: beyond the halide ion diffusion and metal diffusion, *Chemical Engineering Journal* (2023), doi: https://doi.org/10.1016/j.cej.2023.141405

Probing the stability of perovskite solar cell under working condition through an ultra-thin silver electrode: beyond the halide ion diffusion and metal diffusion

Hao Li,[a] Zheng Yan,[a] Min Li,[a] Xiaoyan Wen,[a] Shuo Deng,[a] Sisi Liu,[a] Wallace C. H. Choy,[b] Lijie Li,[c] Ming-Yu Li,[a,d,e] Haifei Lu[a,*]*

[a] School of Science, Wuhan University of Technology, Wuhan, Hubei 430070, China.

[b] Department of Electrical and Electronic Engineering, The University of Hong Kong, Pokfulam Road, Hong Kong, China.

[c] College of Engineering, Swansea University, Swansea, SA1 8EN, UK.

[d] Yangtzi delta region institute of university of electronic science and technology of china, Huzhou Zhejiang 313098, China.

[e] Donghai Laboratory, Zhoushan Zhejiang 316021, China.

Corresponding Author

Ming-Yu Li - School of Science, Wuhan University of Technology, Wuhan, Hubei 430070, China. Yangtzi delta region institute of university of electronic science and technology of china, Huzhou Zhejiang 313098, China. Email: mingyuli.oliver@gmail.com

Haifei Lu - School of Science, Wuhan University of Technology, Wuhan, Hubei 430070, China. Email: haifeilv@whut.edu.cn

Highlights

- In-suit indicator of Ag electrode to inspect degradation of perovskite solar cells.
- Observation of stability evolution of two type devices under different conditions.
- Revealing the interaction process of accumulated charges and movable I^- defects.

ABSTRACT

Perovskite solar cells (PSCs) with an excellent optoelectronic performance have intrigued mushrooming research interests, and the undesirable intrinsic stability of halide perovskite materials still remains a severe constraint for their practical application. Fortunately, the ambiguous and complicated incentives for the degradation process of PSCs under working condition can be directly reflected on the corrosion of silver electrode by halogens. Here, a new perspective for evaluating the long-term stability of PSCs is presented by the time-dependent transverse resistance of the ultrathin silver electrode under different working conditions. Being anode or cathode, the stability of ultra-thin silver layer has been systematically investigated through adjusting the external operating conditions of devices, i.e. light illumination and bias voltage. Experimental results indicate that the gradual resistance increases of silver film can be attributed to the oxidation of I^- existing on the top surface of perovskite layer by non-equilibrium holes generated from light illumination or electrical injection for producing corrosive I_2 gas, which will diffuse through the carrier transporting layer and attack the thin silver layer. The interaction probability of I^- and non-equilibrium holes at the interface plays a critical role on the generation of I_2 gas and resistance variation of the top thin silver electrode. The stability study of electrode indicator will shed light on the ambiguous degradation

mechanisms of PSC under working condition, paving a path for conquering the fatal problems of the practical application.

KEYWORDS: Perovskite solar cell; Metal electrode; Stability; Ion migration.

1. Introduction

Halide perovskites have been into the limelight during the past decade because of their excellent photoelectric properties, including tunable band gap, large absorption coefficient, small exciton binding energy, long carrier diffusion length, efficient photogeneration of free carrier and high charge carrier mobility, which are of great potential for the fabrication of high-performance optoelectronic devices.[1-8] One of the essential challenges has still remained for the long-term stable performance of the halide perovskite optoelectronic devices, originating from the undesirable phase transition and stochiometric variation of perovskites due to their vulnerability to oxygen, moisture, and light illumination.[9] The chemically induced decomposition caused by environmental factors can be efficiently mitigated by the application of perovskite material engineering and encapsulation technique, while relatively weaker chemical bonding in the perovskite lattice is prone to induce the spontaneous ion migration under light irradiation and electric field.[10] Among perovskite optoelectronic applications, photovoltaic devices, especially for perovskite solar cells (PSCs), have gone through rapid development from 2009 to nowadays with a significantly improved power conversion efficiency (PCE) from 3.8% to over 25%.[11-13] Up to date, nearly all of PCSs are fabricated with metal electrode as back contact owing to its high reflectance, suitable work function, and

strong charge collecting ability. However, a large number of studies have claimed that halogens from perovskite are fatal to metal electrode under continuous light illumination and electrical bias for a long time. [14-18] Namely, electrode corrosion can be directly determined by the complex dynamic equilibrium of ion migration and photo-generated carrier diffusion within PCS, correspondingly providing an indicator to the time dependent deterioration of the device.

To ascertain working condition effects, the researches have simplified the model of either a single condition of light irradiation or electrical bias based on a basic structure of metal/perovskite/metal, and experimental results showed that metal electrode was corroded by directional migration of halide ions under potential gradient originated from diffusion of photo-generated carriers or external bias.[19-24] Under the combined conditions of light and heat, the perovskite film was found to be decomposed into PbI_2 and I_2, which accelerated the decomposition.[25-30] Moreover, the stability study for a device with and without counter electrodes in dark nitrogen atmosphere was carried out, and the results indicated that iodine exhaustion in the perovskite layer was produced with the formation of AgI when using Ag electrodes. A hypothesis was put forward that iodine was dislocated by the electric field between the electrodes, and this was an intrinsic cause for migration of I^- from the perovskite until it reaches the anode.[31] Meanwhile, the other explanation on the stability of Ag electrode was mostly attributed to the spontaneous diffusion of silver atoms through the interface layer to the perovskite film when the device was stored in vacuum or dry air.[32, 33] Although the perovskite degradation and electrode corrosion mechanism have been revealed to some degree, the comprehensive understanding on the relationship between metal electrode corrosion and

full device stability is absent and necessary for the practical application of perovskite photoactive devices.

In this paper, taking a typical perovskite solar cell ($MAPbI_3$ PSC) as an example, the time-dependent relationship between Ag electrode corrosion and complex dynamic ion and carrier migration equilibria under different electrical bias and illumination conditions is systematically discussed. Under each condition, the underlying mechanisms involving the accumulation of non-equilibrium charge carriers and I^- at the top surface of perovskite film have been proposed for understanding the different corrosion process within the regular meso-structure and inverted planar structure. The stability characterization strategy and proposed corrosion mechanism presented in this paper are of great interests to the research community concerning the stability study and development of perovskite photoactive devices.

2. Result and discussion

2.1 Continuous light illumination effect

In order to monitor the transverse resistance variation of Ag electrode in perovskite solar cells (PSC) under different conditions, the fresh samples of regular meso-structure and inverted planar device were fabricated for testing. As shown in Figure 1(a) and S1(a), configurations of the regular and inverted device are witnessed with cross-sectional SEM images. The energy level diagrams of the devices are given in Figure 1(b) and Figure S1(b), depicting the migration of electron and hole in absence of bias and light. As shown in Figure 1(c), the as-fabricated film quality of $MAPbI_3$ is evidenced with the uniform distribution of each element, suggesting a good reference for the investigation on the device stability. The plots of current density versus

voltage curve of the as-fabricated regular and inverted devices were recorded in light and dark states, and the photoelectric conversion efficiency under forward and reverse voltage scans was ~12% (Figure S2). The as-prepared sample was quickly transferred from the glove box to a sealed chamber filled with dry nitrogen. A quartz windows was on top of the chamber allowing the device to be exposed to light illumination or keeping the chamber in dark. As the resistance of silver electrode is inverse proportional to the cross-section area of the layer, larger variation of the resistance can be monitored for the electrode with smaller thickness during the corrosion process. As showed in Figure 1(d) and Figure S1(c), two strips of ultra-thin silver electrodes (thickness ~20 nm, length ~1.55 cm, width ~0.40 cm) were fabricated on the device as electrical indicator for reflecting its corrosion. One of the electrodes was the control electrode, whose back side was covered with thick black tape to avoid the light illumination to this electrode. The other electrode was connected with a steady voltage source, providing a constant electrical bias between the top electrode and bottom transparent conductive oxide (TCO) during the characterization process. An additional source meter was connected to electrical probes, which were mounted on the two ends of the thin silver layer, for recording the time dependent resistance variation and characterizing the stability of electrode. To avoid misunderstanding, we stipulated that the electrode adjacent to the holes transporting layer (HTL) has higher potential under forward bias, and the electrode adjacent to the electrons transporting layer (ETL) has higher potential under reverse bias correspondingly. Figure S3 shows the transverse resistance variation of control Ag electrodes on regular and inverted device when the samples were kept open circuit and stored in the dark environment for 96 hours. R_0 represents the origin resistance, and R represents the time-dependent resistance. Experimental results indicated that

thin silver layer on the regular and inverted device under the open-circuited and dark condition experienced a negligible resistance increase. Therefore, a same normalized resistance variation of control electrode has been adopted for characterizing the resistance variation of thin silver electrode on the identical device to minimize the error from different batch of device fabrication.

For the stability study of Ag under single condition of light illumination, the regular and inverted structures of photovoltaic device with thin silver layer on top were firstly short-circuited or open-circuited under light illumination. As the results shown in Figure 1(e), quite different stability performance of the Ag electrodes was observed. The thin silver layer in the open-circuited regular device experienced a rapid resistance increase after 9 hours continuous light irradiation (R_{RO}), and a relatively negligible resistance increase was observed for the electrode in short-circuited device after 11 hours irradiation (R_{RS}). In contrast, the thin silver electrodes in short-circuited and open-circuited inverted devices all experienced small resistance (R_{IO} and R_{IS}) increases after 11 hours light illumination, and a slight larger resistance increase was observed for the electrode in short-circuited device than the one in open-circuited device.

To understand the different stability of thin silver layer on different structure of devices under light irradiation, the upper surface of perovskite film or the upper interface of perovskite and charge transporting layer, which is close to the top electrode of thin silver film, will be majorly discussed. It is also well acknowledged that the surface and grain boundary of perovskite film generally possess much larger defect concentration than the one in the perovskite crystal. The

unbonded I^-, which have been demonstrated to be movable on the grain boundary, [34] will incline to capture the free charge carrier of holes and be oxidized into I_2. Based on this assumption, the stability variation of thin silver electrode on different devices can be understood, and the schematic illustration is depicted in Figure 2(a) and (b). For the regular solar cell structure of FTO/c-TiO_2/m-TiO_2/$MAPbI_3$/spiro-OMeTAD/Ag, $MAPbI_3$/spiro-OMeTAD interface will be majorly considered and the c-TiO_2/m-TiO_2 layer has been simplified into one layer in the schematic diagram. Under the dark and open circuit conditions, a space charge region with almost no internal carriers was formed at the interface of normal device, [35] and the surface of perovskite layer containing massive I^- was also included in this region. Thus, less hole can be provided for the oxidation of I^-, and the silver electrode kept relatively stable as shown in Figure S3(a). The similar reason can be attributed to the ignorable resistance increase of thin silver electrode in the inverted structure of ITO/PEDOT: PSS/$MAPbI_3$/PCBM/BCP/Ag under the dark and open circuit conditions as shown in Figure S3(b).

For the regular device illuminated with light, great amount of photo-induced charge carriers was generated in the perovskite film, which separately diffused to the two opposite interfaces of perovskite layer, and resulted in the vanish of space charge region. When the regular device was open-circuit, large quantity of holes accumulated at the interface of $MAPbI_3$/spiro-OMeTAD, which tended to easily capture by I^- for generating I_2 gas. The highly corrosive I_2 gas will diffuse through the pinholes of HTL to the bottom surface of ultra-thin silver film, inducing corrosion and rapid resistance increase of the top metal electrode, which has been demonstrated by XPS (X-ray photoelectron spectroscopy) results in Figure S4 (a) and (b).

Meanwhile, the photo-generated holes were quickly extracted to the cathode and recombined with the electrons from anode when the device was short-circuited, which in turn reduced the interaction probability between holes and I^- at the interface. Therefore, the top electrode in the short-circuited regular device exhibited a relatively better stability under 11 hours constant light irradiation. For the inverted device under open circuit and light illumination condition, the accumulated charge carriers on the top interface of $MAPbI_3$/PCBM were electrons, which in contrary stabilized I^- on the perovskite surface. The interaction chance between holes and I^- at the top interface of perovskite/ETL was still small, even when inverted device was short-circuited and exposed to light illumination. As shown in Figure S4 (c), XPS results indicated Ag electrodes had not been corroded. The slight resistance increase of the thin silver electrode was majorly attributed to the diffusion of silver atom into the charge transporting layer. [36]

Furthermore, the morphological characteristics were further characterized by atomic force microscopy (AFM) under the tapping-mode at room temperature. As shown in Figure 2(c), the root-mean-squared roughness (R_{RMS}) of $MAPbI_3$ film slightly increased after light illumination regardless of the configuration. To further verify the hypothesis, carrier dynamics information of $MAPbI_3$ film in both regular and inverted structure were recorded with the time resolved PL (TRPL) spectra. As shown in Figure 2(d), the τ_{avg} of two devices decreased by 57.69% and 21.52%, and the sharp decrease in carrier lifetime indicated that there were more defects in the regular structure of perovskite film than in the inverted structure after exposure to light, which can be possibly resulted from additional defect formation along with the oxidation of I^-. [37]

2.2 Applied electrical bias effect

To investigate the electrical bias effect on the deterioration in the conductivity of Ag electrode, another batch of devices were stored in dark environment and applied with different voltage of forward or reverse bias. As shown in Figure 3(a) and (b), both electrodes in the two kinds of photovoltaic device exhibited a bias dependent resistance variation along with different trends. For the regular device, the larger forward electrical bias, the faster resistance increase has been observed for the top silver electrode at the beginning of applying bias. Large reverse electrical bias applied on the regular device can help to stabilize the thin silver electrode, which was however opposite to the results from the electrode in the inverted device applied with reverse bias. In the inverted device applied with forward bias, the thin silver electrode maintained stable with relatively less resistance increase. It was also noticed that the resistance increases of electrode in regular device applied with forward bias, i.e. 1.0 V, was more severe than the electrode in inverted device applied with reverse bias, i.e. -1.0 V.

Similar mechanism involving the interaction of non-equilibrium charge carrier and I^- at the top surface of perovskite film can be used for the interpretation of two kinds of device under electrical bias and dark condition. For the regular device applied with forward bias as shown in Figure 3(c)-i and 3(c)-ii, the thickness of space charge region shrunk due to the opposite direction of external bias and the internal built-in potential, which was vanished eventually when the applied voltage exceeded the V_{oc} of the device. In this case, I^- on perovskite film has more chance to be oxidized by holes diffused from HTL, AgI was detected in the Ag electrodes (Figure S5 (a) and (b)). Otherwise, as shown in Figure 3(c)-iii, with the increased reverse external bias, the space charge region was broadened, which on one hand elongated the distance between holes from HTL and I^- on the perovskite film surface. On the other hand, the

intensified built-in field in the space charge region drove the negative charged I^- into the perovskite film. Both of the two effects contributed to the mild resistance variation with the increased reverse bias as demonstrated in Figure 3(a).

In addition, the inverted structure with Ag electrode as cathode under different external bias is presented by the schematic diagram shown in Figure 3(d). Similarly, the forward bias applied on the inverted structure of solar cell also narrowed down the space charge region, which however allowed the diffusion of electrons from ETL to perovskite layer. As more electrons diffused through the interface of perovskite/ETL, the probability of I^- oxidation by holes is decreased for the device under forward bias. For the inverted device, the broadening of space charge region and strengthened built-in electrical field can be expected with increased reverse voltages. As the direction of built-in electrical field was from ETL to perovskite layer, the movable I^- in the perovskite film were driven to high potential through the path of grain boundary. Correspondingly, it induced the accumulation of more I^- at the interface of perovskite/ETL, some of which will capture holes and be oxidized into I_2 gas to corrode the top thin silver layer, the existence of AgI was confirmed by XPS in Figure S5 (c) and (d). Since the holes in space charge region of the inverted device under reverse bias were much less than the holes diffused through the perovskite/HTL of the regular device under forward bias, the different degree of resistance increase was obtained as evidenced in Figures 3(a) and 3(b).

The first principle calculation of binding energies between I^- and perovskite surface with different kinds of doping has been carried out to explain the oxidation of I^- under different conditions. To mimic the situation of electron and hole accumulation, the atomic structures

models of intrinsic, P-type and N-type $MAPbI_3$ were constructed, and the corresponding simulated band diagrams are represented in Figure 4. The atom binding energy (E_b) between I atom and perovskite interface are defined as the energy required to form the compound cell from individual atoms $E_b = E_{system} – E_I – E_{MAPbI3}$, where Esystem is the calculated total energy of I atom bonded $MAPbI_3$ interface, E_I and E_{MAPbI3} are calculated energies of I atom and $MAPbI_3$ (N-type or P-type) interface respectively. According to the simulation, the binding energy between I^- and $MAPbI_3$ with holes as majority carriers was 156.5 meV lower than that between I^- and $MAPbI_3$ with electrons as majority carriers, suggesting that extra holes can radically intensify adsorption of iodine ions for the oxidation.

2.3 Comprehensive influence under light and bias conditions

In practice, light illumination and applied bias are commonly believed as coexisting work conditions for PSCs, and the synthetic condition effect was studied on the forward-structure device as depicted in Figure 5(a). As clearly shown in Figures 5(b) and 5(c), a sharp comparison in surface morphology of the as-prepared Ag electrode and the one after 11 hours testing was observed with the occurrence of nanoparticles and nanoholes on the Ag electrode. In addition, morphological development of perovskite layer before and after test was also studied through removing the thin silver film and spiro-OMeTAD layer. As shown in Figure 5(d), the perovskite layer before test was witnessed with an outstanding continuity, and the morphology became rugged and porous as revealed in Figure 5(e). Similarly, the deterioration in surface morphology appeared for the Ag electrode and perovskite layer of the device with inverted configuration as shown in Figure S4. According to the theoretical mechanism of the two

conditions derived above, a mechanism of electrode corrosion under both light and bias conditions can be assumed. As the schematic diagrams shown in Figure 5(f), under light irradiation and forward bias, the separation and extraction of photo-induced carriers were restrained, and thus the photo-generated holes tended to accumulate at perovskite/HTL interface. When the forward bias increased further, the external charges of holes began to inject from the anode into perovskite layer, leading to a large number of holes passing through I^- on the interface. Therefore, more I_2 were generated as shown in Figure 5(f)-i and 5(f)-ii. To subsequent, I_2 spontaneously diffused through the polymer film of spiro-OMeTAD, and the intensified corrosion of Ag electrode can be correspondingly expected as explained below,

$$2I^- + 2h^+ = I_2 \quad (1)$$

$$2Ag + I_2 = 2AgI \quad (2)$$

Meanwhile, the diffusion of Ag atoms through the spiro-OMeTAD concurrently happened. Correspondingly, the oxidation process at the interface of $MAPbI_3$/spiro-OMeTAD was further enhanced as explained with the related formulas below,

$$Ag + I^- + h^+ = AgI \quad (3)$$

For the device under light and reverse bias, the distribution charge carriers and I^- are depicted in Figure 5(f)-iii. Electrons and holes from external circuit were injected into perovskite layer from spiro-OMeTAD and TiO_2, recombining with photo-induced holes and electrons respectively, which reduced the encounter chance of the photo-generated holes and iodine ions.

The corrosion mechanism of Ag electrode in inverted structure device under light and reverse bias is clearly illustrated in Figure 5(g). Under forward bias and light irradiation, part of the photo-generated electrons accumulated at the perovskite/ETL interface of the inverted device, and the accumulation of electrons became radical with external electrical injection at the increased forward bias as shown in Figure 5(g)-i and ii. Consequently, I^- on top surface of perovskite layer were passivated by the electrons, suppressing the oxidation of I^-. Therefore, the Ag electrode exhibited a better stability under forward bias. As show in Figure 5(g)-iii, the intensified built-in field was beneficial to the separation and extraction of photo-induced electrons and holes to ETL and HTL at reverse bias, which however drove the motion of I^- from perovskite film to perovskite/ETL interface. The increased amount of I^- recombined with the photo-induced holes at sub-surface of perovskite film and oxidized into I_2. As a result, the diffusion of I_2 gas accelerated the decomposition of perovskite film and the corrosion to Ag electrode.

To verify the mechanism, the characterization on resistance also applied in the two types of devices under both light and bias. These experimental results were consistent with the previous characterization and mechanism, as shown in Figure 6(a) and 6(b). For the regular structure, when light and forward bias were concurrently applied on the device, similar resistance variation tendency to the device applied with electrical bias was observed. Whereas, the increase ratio of resistance from the sample under bias and light irradiation was higher than the ratio from the sample only under bias condition. That can be attributed to the generation of photo-induced charge carriers under light irradiation and more holes were provided to be captured by I^-. Despite the space charge region of regular device was broadened under reverse

bias, photo-generated charge carriers can be also produced in this region, and the I^- captured a small portion of holes for generating small amount of I_2 gas. It is also necessary to mention that a slightly larger resistance increase of the electrode under reverse bias and light irradiation than the electrode under merely reverse bias, which can be induced by the generation of hole-electron pairs in the whole perovskite film under light irradiation. The time-dependent transvers resistance variation of Au electrodes-based regular device under light irradiation and 1.5 V forward bias had been carried out as a comparison with Ag (Figure S7). In contrast to Ag electrode, Au electrode showed very high stability and less corrosion had been observed (Figure S7 (a)). However, the sharp decline in the performance of the device (Figure S7 (b)) indicates that the device itself had undergone the decomposition as described above.

To provide a solid evidence, XRD and XPS were adopted to analyze the crystal structure and element state of the samples before and after electrical characterization. As shown in Figure 6(c) (regular device) and Figure S8 (inverted device), noticeable peaks of $MAPbI_3$ and Ag were equally observed with the as-prepared regular and inverted devices. For the device after 11 hours electrical characterization, the intensity of diffraction peak from Ag film was decreased and a sharp peak of AgI was observed, confirming the severe corrosion by I_2 gas diffused from the perovskite layer. There was no obvious diffraction peak of AgI occurred for the device after removal of Ag/HTL layer, indicating the diffused silver atom to the perovskite layer was too less to form detectable amount of AgI crystal. In addition, XPS results confirmed the existence of AgI in the sample after electrical characterization. Figure 6(d) shows the normalized binding energy peaks of Ag 3d. For the fresh sample, Ag electrode displayed the binding energy peaks at 368.2 eV and 374.2 eV, representing the only component of metal Ag. After 11 hours

electrical characterization with 1.5 V bias and light irradiation, the binding energy peaks of the top electrode shifted towards lower energies of 367.8 eV and 373.8 eV, indicating the oxidation of the thin silver layer. For the sample with the removal of Ag and HTL after electrical characterization, weak signal of Ag peak was detected on the surface of perovskite film. It suggested that a small amount of Ag can diffuse through HTL into perovskite layer, which was also oxidized as the binding energy peaks shifted towards lower energies as well. Also, the normalized binding energy peaks of I 3d indicate I combined Ag after electrical and light illumination characterization (Figure S9). The same thing happened with inverted device (Figure S10).

Based on our experimental observation, the undesired generation of gas state of I_2, due to oxidation of movable I^- defects with the accumulated holes at the interface, is a major cause of the corrosion of silver electrode. Both of degradation of perovskite film and the silver electrode are negative to the stability of perovskite solar cells. The first and important suggestion for improving the device stability is to reduce or avoid the formation I_2 gas, which can be solved by minimizing the defects in perovskite film and avoiding the charge carriers' accumulation at the interface. Improving the film quality and passivating the defects on perovskite film can be the effective approach to reduce and stabilize the defects, and improving the extraction and transportation of photo-induced charge carriers through the interface can effectively reduce the accumulation of charge carriers. Selecting the perovskite material with high stability for optoelectronic device is the ultimate solution. The second suggestion is to prevent the diffusion of I_2 gas toward the silver electrode for protecting the electrode, which can be solved through introduction of block layers and material selection. The third suggestion is to use the

anticorrosive electrode, such as anti-corrosive metal, metal oxide electrode and carbon-based electrode, to minimize the negative effect brought by electrode degradation.

3. Conclusion

In conclusion, the stabilities of regular and inverted structures of PSC under single condition or both conditions of light illumination and bias voltage have been respectively inspected through adopting ultra-thin Ag layer as an electrical indicator. Both of light irradiation and forward bias promote the corrosion of Ag electrode on the regular structure of perovskite device as proven by the resistance variation of top silver electrode, while reverse bias suppresses the corrosion process against the anode. Differently, reverse bias on the inverted structure of perovskite device promote the corrosion of top silver cathode. The mechanism behind the different phenomena is proposed to the interaction between I^- on perovskite surface and non-equilibrium carrier, which is also suitable to explain the completely different results of regular and inverted solar cells under both light irradiation and electrical bias. The I^- at interface of perovskite and transporting layer will capture photo-induced holes and external holes injected from transporting layer under electrical bias, which will be oxidized into I_2 to corrode the top electrode of ultra-thin silver layer. On the contrary, the accumulation of electrons from photo-generation or external electrical injection at the top interface will passivate I^- from oxidation and cause less resistance increase of the metal electrode. Based on the experimental observation and the proposed mechanism, reducing or passivating defects at the interface and efficient extraction of photo-induced charges will be beneficial to the stability of perovskite devices. The study of different interfaces in perovskite solar cells under working

conditions presented in this paper will provide guidance for understanding the stability issues of optoelectronic devices based on perovskite materials.

4. Experimental section

4.1 Preparation of Regular Meso-structure Device

The substrates of FTO were ultrasonic cleaned in detergent, deionized water, acetone and ethanol for 20 mins respectively. Then, FTO substrates were treated with UV-Ozone for 20 mins. Subsequently, a thin layer of compact-TiO_2 (c-TiO_2) was prepared on FTO surface through spin-coating proper amount of precursor (titanium diisopropoxide bis-acetylacetonate dissolved in ethanol with volume ratio of 1:19) at 4000 rpm for 20 s, followed by heating at 150 ℃ for 10 mins and thermal annealing in air at 500 ℃ for 30 min. The mesoporous-TiO_2 (m-TiO_2) layer (TiO_2 nanoparticle paste dissolved in ethanol with weight ratio of 1:5) was deposited on the c-TiO_2 layer by spin-coating at 3500 rpm for 20 s, heated at 150 ℃ for 10 min, and then annealed at 500 ℃ for 30 min in air. The fabrication of perovskite film on FTO/c-TiO_2/m-TiO_2 substrates was carried out in the N_2-filled glovebox according to anti-solvent approach.[38] Perovskite (170 nm) precursor (1.2 M, by mixing 0.5532 g PbI_2 and 0.1908 g MAI into 0.7 mL γ-butyrrolactone and 0.3 mL dimethyl sulfoxide) was dropped on the substrate and spin-coated via a two-step process. The first step is 1000 rpm for 10 s, and the second step is 4000 rpm for 30 s. A proper amount of methylbenzene as anti-solvent was dropped on the substrate during the second step, which was then annealed at 100 ℃ for 10 min. Then, 72.3 mg/mL of spiro-OMeTAD (50 nm) solution (dissolved in chlorobenzene) mixed with 17.5 μL LiTFSI solution (dissolved in acetonitrile) and 28.8 μL TBP was deposited on the

surface of perovskite film at 4000 rpm for 30 s. Finally, the back contact of regular PSC device was achieved by thermal evaporating two strips of 20 nm Ag layer through a mask.

4.2 Preparation of Inverted Planar Device

ITO were ultrasonic cleaned in detergent, deionized water, acetone and ethanol for 20 min respectively. Then, the ITO substrates were treated with UV-Ozone for 20 mins. Subsequently, a thin layer of PEDOT:PSS was deposited on the ITO electrode by spin-coating at 4000 rpm for 30 s, followed by heating at 125 ℃ for 15 mins. The preparation of perovskite layer on ITO/PEDOT:PSS substrate was also carried out in the N_2-filled glovebox and followed the same protocol as mentioned above. The electron transporting layer was prepared on perovskite film through spin-coating 17 mg/mL of PCBM (40 nm) solution (dissolved in chlorobenzene) at 1500 rpm for 30s. Subsequently, 0.06 mg/mL of BCP solution (dissolved in isopropanol) was spin-coated at 3000 rpm for 60s. Finally, two strips of 20 nm Ag layer were evaporated as top electrodes.

4.3 Characterization of Thin Electrode Based Devices

The fresh prepared sample was quickly transferred to a sealed chamber.[39] Before executing the electrical characterization of the top electrode under specific environmental conditions, the chamber was quickly exhausted to vacuum and inlet dry N_2 for several times to remove the remained O_2 and H_2O, which was finally filled with dry N_2 in a standard atmosphere pressure. On top of the chamber, a quartz window can allow the sample to be exposed from glass substrate by 1 sunlight from a solar simulator during the electrical characterization of the metal electrode on device. A steady voltage source was connected with the cathode and anode

for loading different electrical bias on device. The resistance variation of metal electrode was recorded consistently by Keithley 2400 source meter. Morphology studies of the samples were characterized by using field-emission scanning electron microscope (SU8010, Hitachi), and the atomic force microscopy (Dimension Icon, Bruker). Time-resolved PL spectra were measured by TCSPC (FLS1000, Edinburgh) equipped with a 375 nm picosecond pulse laser. The samples after electrical characterization were further characterized by XRD (Empyrean) and XPS (ESCALAB 250Xi) to investigate the chemical composition and chemical state.

CRediT authorship contribution statement

Ming-Yu Li and **Haifei Lu** participated in the experiment design and carried out the experiments. **Hao Li**, **Zheng Yan**, **Xiaoyan Wen**, **Min Li**, **Wallace C. H. Choy** and **Lijie Li** participated in the analysis of date. **Zheng Yan** and **Haifei Lu** designed the experiments and testing methods. **Hao Li**, **Ming-Yu Li** and **Haifei Lu** carried out the writing of the manuscript. All authors helped in drafting and reading and approving the final manuscript.

Declaration of Competing Interest

The authors declare that they have no known competing financial interests or personal relationships that could have appeared to influence the work reported in this paper.

Acknowledgements

The research was supported by National Key R&D Program of China (2021YFF0603500), National Natural Science Foundation of China (NSFC 11974266, 11704293, 62075174), Fundamental Research Funds for the Central Universities (WUT: 2021III063JC, 2020IB004,

2021VA056, 2022IVA061) and Science Foundation of Donghai Laboratory (DH-2022KF01007).

5. References

[1] C. C. Stoumpos, M. G. Kanatzidis, The Renaissance of Halide Perovskites and Their Evolution as Emerging Semiconductors, Acc. Chem. Res. 48 (2015) 2791-2802. https://doi.org/10.1021/acs.accounts.5b00229.

[2] M. A. Green, A. Ho-Baillie, H. J. Snaith, The Emergence of Perovskite Solar Cells, Nat. Photonics 8 (2014) 506-514. https://doi.org/10.1038/nphoton.2014.134.

[3] C. S. Ponseca, T. J. Savenije, M. Abdellah, K. Zheng, A. Yartsev, T. Pascher, T. Harlang, P. Chabera, T. Pullerits, A. Stepanov, J.-P. Wolf, V. Sundström, Organometal Halide Perovskite Solar Cell Materials Rationalized: Ultrafast Charge Generation, High and Microsecond-Long Balanced Mobilities, and Slow Recombination, J. Am. Chem. Soc. 136 (2014) 5189-5192. https://doi.org/10.1021/ja412583t.

[4] Q. Dong, Y. Fang, Y. Shao, P. Mulligan, J. Qiu, L. Cao, J. Huang, Electron-Hole Diffusion Lengths > 175 MM in Solution-Grown $CH_3NH_3PbI_3$ Single Crystals, Science 347 (2015) 967-970. https://doi.org/10.1126/science.aaa5760.

[5] G. Kim, H. Min, S. Lee Kyoung, Y. Lee Do, M. Yoon So, I. Seok Sang, Impact of Strain Relaxation on Performance of α-formamidinium Lead Iodide Perovskite Solar Cells, Science 370 (2020) 108-112. https://doi.org/10.1126/science.abc4417.

[6] A. Al-Ashouri, E. Köhnen, B. Li, A. Magomedov, H. Hempel, P. Caprioglio, A. Márquez José, B. Morales Vilches Anna, E. Kasparavicius, A. Smith Joel, N. Phung, D. Menzel, M. Grischek, L. Kegelmann, D. Skroblin, C. Gollwitzer, T. Malinauskas, M. Jošt, G. Matič, B. Rech, R. Schlatmann, M. Topič, L. Korte, A. Abate, B. Stannowski, D. Neher, M. Stolterfoht, T. Unold, V. Getautis, S. Albrecht, Monolithic Perovskite/Silicon Tandem Solar Cell with >29% Efficiency by Enhanced Hole Extraction, Science 370 (2020) 1300-1309. https://doi.org/10.1126/science.abd4016.

[7] K. Lin, J. Xing, L. N. Quan, F. P. G. de Arquer, X. Gong, J. Lu, L. Xie, W. Zhao, D. Zhang, C. Yan, W. Li, X. Liu, Y. Lu, J. Kirman, E. H. Sargent, Q. Xiong, Z. Wei, Perovskite Light-Emitting Diodes with External Quantum Efficiency Exceeding 20 Percent, Nature 562 (2018) 245-248. https://doi.org/10.1038/s41586-018-0575-3.

[8] J. Zhao, L. Zhao, Y. Deng, X. Xiao, Z. Ni, S. Xu, J. Huang, Perovskite-Filled Membranes for Flexible and Large-Area Direct-Conversion X-Ray Detector Arrays, Nat. Photonics 14 (2020) 612-617. https://doi.org/10.1038/s41566-020-0678-x.

[9] H. Zai, Y. Ma, Q. Chen, H. Zhou, Ion Migration in Halide Perovskite Solar Cells: Mechanism, Characterization, Impact and Suppression, J. Energy Chem. 63 (2021) 528-549. https://doi.org/10.1016/j.jechem.2021.08.006.

[10] J.-W. Lee, S.-G. Kim, J.-M. Yang, Y. Yang, N.-G. Park, Verification and Mitigation of Ion Migration in Perovskite Solar Cells, APL Mater. 7 (2019) 041111. https://doi.org/10.1063/1.5085643.

[11] A. Kojima, K. Teshima, Y. Shirai, T. Miyasaka, Organometal Halide Perovskites as Visible-Light Sensitizers for Photovoltaic Cells, J. Am. Chem. Soc. 131 (2009) 6050-6051. https://doi.org/10.1021/ja809598r.

[12] J.-H. Im, C.-R. Lee, J.-W. Lee, S.-W. Park, N.-G. Park, 6.5% Efficient Perovskite Quantum-Dot-Sensitized Solar Cell, Nanoscale 3 (2011) 4088-4093. https://doi.org/10.1039/C1NR10867K.

[13] M. Kim, G.-H. Kim, T. K. Lee, I. W. Choi, H. W. Choi, Y. Jo, Y. J. Yoon, J. W. Kim, J. Lee, D. Huh, H. Lee, S. K. Kwak, J. Y. Kim, D. S. Kim, Methylammonium Chloride Induces Intermediate Phase Stabilization for Efficient Perovskite Solar Cells, Joule 3 (2019) 2179-2192. https://doi.org/10.1016/j.joule.2019.06.014.

[14] H. Lu, X. Ren, D. Ouyang, W. C. H. Choy, Emerging Novel Metal Electrodes for Photovoltaic Applications, Small 14 (2018) 1703140. https://doi.org/10.1002/smll.201703140.

[15] D. S. Hecht, L. Hu, G. Irvin, Emerging Transparent Electrodes Based on Thin Films of Carbon Nanotubes, Graphene, and Metallic Nanostructures, Adv. Mater. 23 (2011) 1482-1513. https://doi.org/10.1002/adma.201003188.

[16] H. Lu, D. Zhang, J. Cheng, J. Liu, J. Mao, W. C. H. Choy, Locally Welded Silver Nano-Network Transparent Electrodes with High Operational Stability by a Simple Alcohol-Based Chemical Approach, Adv. Funct. Mater. 25 (2015) 4211-4218. https://doi.org/10.1002/adfm.201501004.

[17] J.-W. Xiao, C. Shi, C. Zhou, D. Zhang, Y. Li, Q. Chen, Contact Engineering: Electrode Materials for Highly Efficient and Stable Perovskite Solar Cells, Sol. RRL 1 (2017) 1700082. https://doi.org/10.1002/solr.201700082.

[18] L. Liang, Y. Cai, X. Li, M. K. Nazeeruddin, P. Gao, All That Glitters Is Not Gold: Recent Progress of Alternative Counter Electrodes for Perovskite Solar Cells, Nano Energy 52 (2018) 211-238. https://doi.org/10.1016/j.nanoen.2018.07.049.

[19] Y. Yuan, J. Chae, Y. Shao, Q. Wang, Z. Xiao, A. Centrone, J. Huang, Photovoltaic Switching Mechanism in Lateral Structure Hybrid Perovskite Solar Cells, Adv. Energy Mater. 5 (2015) 1500615. https://doi.org/10.1002/aenm.201500615.

[20] Y. Yuan, Q. Wang, Y. Shao, H. Lu, T. Li, A. Gruverman, J. Huang, Electric-Field-Driven Reversible Conversion Between Methylammonium Lead Triiodide Perovskites and Lead Iodide at Elevated Temperatures, Adv. Energy Mater. 6 (2016) 1501803. https://doi.org/10.1002/aenm.201501803.

[21] C. Li, S. Tscheuschner, F. Paulus, P. E. Hopkinson, J. Kießling, A. Köhler, Y. Vaynzof, S. Huettner, Iodine Migration and its Effect on Hysteresis in Perovskite Solar Cells, Adv. Mater. 28 (2016) 2446-2454. https://doi.org/10.1002/adma.201503832.

[22] S. Bae, S. Kim, S.-W. Lee, K. J. Cho, S. Park, S. Lee, Y. Kang, H.-S. Lee, D. Kim, Electric-Field-Induced Degradation of Methylammonium Lead Iodide Perovskite Solar Cells, J. Phys. Chem. Lett. 7 (2016) 3091-3096. https://doi.org/10.1021/acs.jpclett.6b01176.

[23] Y.-C. Zhao, W.-K. Zhou, X. Zhou, K.-H. Liu, D.-P. Yu, Q. Zhao, Quantification of Light-Enhanced Ionic Transport in Lead Iodide Perovskite Thin Films and Its Solar Cell Applications, Light Sci. Appl. 6 (2017) e16243-e16243. https://doi.org/10.1038/lsa.2016.243.

[24] Y. Yuan, J. Huang, Ion Migration in Organometal Trihalide Perovskite and Its Impact on Photovoltaic Efficiency and Stability, Acc. Chem. Res. 49 (2016) 286-293. https://doi.org/10.1021/acs.accounts.5b00420.

[25] L. Jiang, J. Lu, S. R. Raga, J. Sun, X. Lin, W. Huang, F. Huang, U. Bach, Y.-B. Cheng, Fatigue Stability of $CH_3NH_3PbI_3$ Based Perovskite Solar Cells in Day/Night Cycling, Nano Energy 58 (2019) 687-694. https://doi.org/10.1016/j.nanoen.2019.02.005.

[26] G. Divitini, S. Cacovich, F. Matteocci, L. Cinà, A. Di Carlo, C. Ducati, In Situ Observation of Heat-Induced Degradation of Perovskite Solar Cells, Nat. Energy 1 (2016) 15012. https://doi.org/10.1038/nenergy.2015.12.

[27] E. J. Juarez-Perez, L. K. Ono, M. Maeda, Y. Jiang, Z. Hawash, Y. Qi, Photodecomposition and Thermal Decomposition in Methylammonium Halide Lead Perovskites and Inferred Design Principles to Increase Photovoltaic Device Stability, J. Mater. Chem. A 6 (2018) 9604-9612. https://doi.org/10.1039/C8TA03501F.

[28] F. Liu, Q. Dong, M. K. Wong, A. B. Djurišić, A. Ng, Z. Ren, Q. Shen, C. Surya, W. K. Chan, J. Wang, A. M. C. Ng, C. Liao, H. Li, K. Shih, C. Wei, H. Su, J. Dai, Is Excess PbI_2 Beneficial for Perovskite Solar Cell Performance?, Adv. Energy Mater. 6 (2016) 1502206. https:// doi.org/10.1002/aenm.201502206.

[29] J.Schoonman, Organic–Inorganic Lead Halide Perovskite Solar Cell Materials: A Possible Stability Problem, Chem. Phys. Lett. 619 (2015) 193-195. https://doi.org/10.1016/j.cplett.2014.11.063.

[30] A. Friedenberg, Y. Shapira, Photolysis and Conductivity Measurements at PbI_2 Surfaces, Surf. Sci. 115 (1982) 606-622. https://doi.org/10.1016/0039-6028(82)90391-0.

[31] C. Besleaga, L. E. Abramiuc, V. Stancu, A. G. Tomulescu, M. Sima, L. Trinca, N. Plugaru, L. Pintilie, G. A. Nemnes, M. Iliescu, H. G. Svavarsson, A. Manolescu, I. Pintilie, Iodine Migration and Degradation of Perovskite Solar Cells Enhanced by Metallic Electrodes, The Journal of Physical Chemistry Letters 7 (2016) 5168-5175. https://doi.org/10.1021/acs.jpclett.6b02375.

[32] S. Svanström, T. J. Jacobsson, G. Boschloo, E. M. J. Johansson, H. Rensmo, U. B. Cappel, Degradation Mechanism of Silver Metal Deposited on Lead Halide Perovskites, ACS Appl. Mater. Inter. 12 (2020) 7212-7221. https://doi.org/10.1021/acsami.9b20315.

[33] X. Li, H.-h. Ding, G.-h. Li, Y. Wang, Z.-m. Fang, S.-f. Yang, H.-x. Ju, J.-f. Zhu, In Situ Investigations of Interfacial Degradation and Ion Migration at $CH_3NH_3PbI_3$ Perovskite/Ag Interface, Chin. J. Chem. Phys. 32 (2019) 299-305. https://doi.org/10.1063/1674-0068/cjcp1808189.

[34] Y. Shao, Y. Fang, T. Li, Q. Wang, Q. Dong, Y. Deng, Y. Yuan, H. Wei, M. Wang, A. Gruverman, J. Shield, J. Huang, Grain Boundary Dominated Ion Migration in Polycrystalline Organic–Inorganic Halide Perovskite Films, Energy Environ. Sci. 9 (2016) 1752-1759. https://doi.org/10.1039/C6EE00413J.

[35] L. Bertoluzzi, C. C. Boyd, N. Rolston, J. Xu, R. Prasanna, B. C. O'Regan, M. D. McGehee, Mobile Ion Concentration Measurement and Open-Access Band Diagram Simulation Platform for Halide Perovskite Solar Cells, Joule 4 (2020) 109-127. https://doi.org/10.1016/j.joule.2019.10.003.

[36] J. Li, Q. Dong, N. Li, L. Wang, Direct Evidence of Ion Diffusion for the Silver-Electrode-Induced Thermal Degradation of Inverted Perovskite Solar Cells, Adv. Energy Mater. 7 (2017) 1602922. https://doi.org/10.1002/aenm.201602922.

[37] T. Kirchartz, J. A. Márquez, M. Stolterfoht, T. Unold, Photoluminescence-Based Characterization of Halide Perovskites for Photovoltaics, Adv. Energy Mater. 10 (2020) 1904134. https://doi.org/10.1002/aenm.201904134.

[38] R. Liu, K. Xu, Solvent Engineering for Perovskite Solar Cells: A Review, Micro Nano Lett. 15 (2020) 349-353. https://doi.org/10.1049/mnl.2019.0735.

[39] Z. Yan, H. Chen, M. Li, X. Wen, Y. Yang, W. C. H. Choy, H. Lu, Observing and Understanding the Corrosion of Silver Nanowire Electrode by Precursor Reagents and $MAPbI_3$ Film in Different Environmental Conditions, Adv. Mater. Inter. 8 (2021) 2001669. https://doi.org/10.1002/admi.202001669.

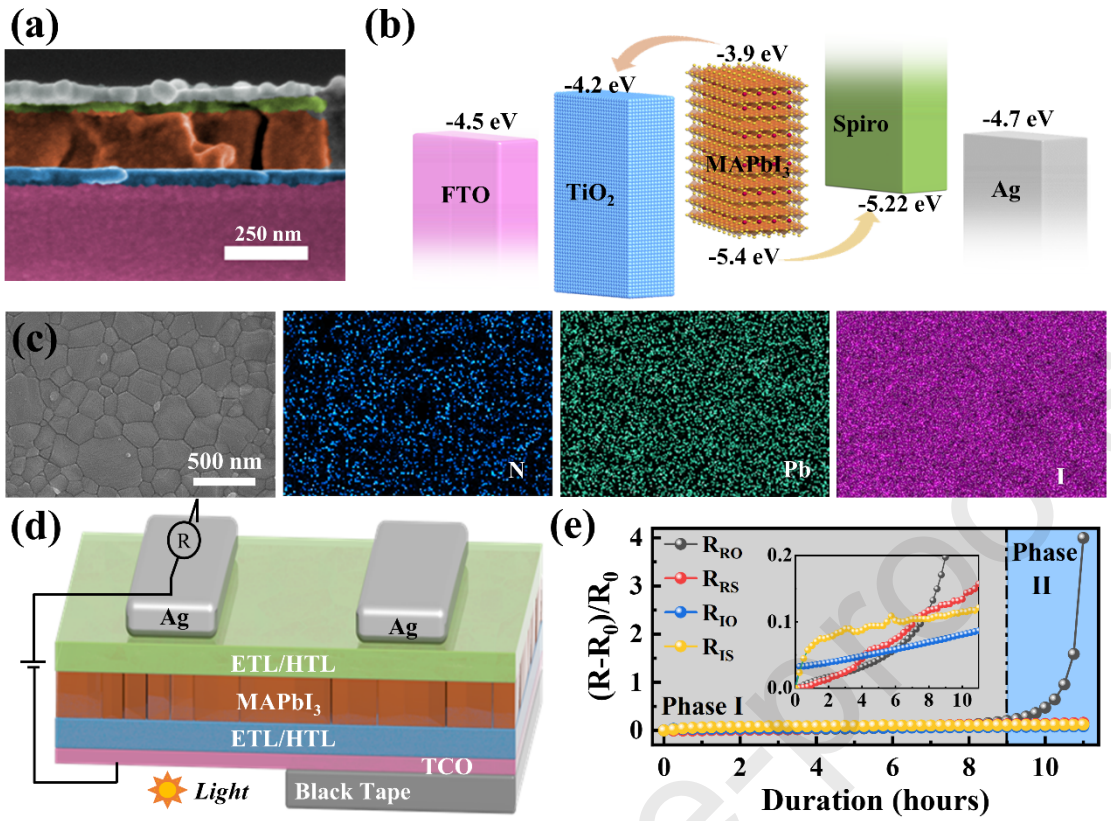

Figure 1. (a) Cross-sectional scanning electron microscope (SEM) image of regular meso-structure device. (b) Energy level diagram of regular meso-structure device. (c) SEM images and energy dispersive X-ray spectroscopy (EDS) maps of $MAPbI_3$ film: blue (N), green (Pb) and purple (I). (d) The electrode stability characterization scheme. (e) The transverse resistance variation of Ag electrode in devices with regular meso-structure and inverted device under light & open circuit or light & short circuit.

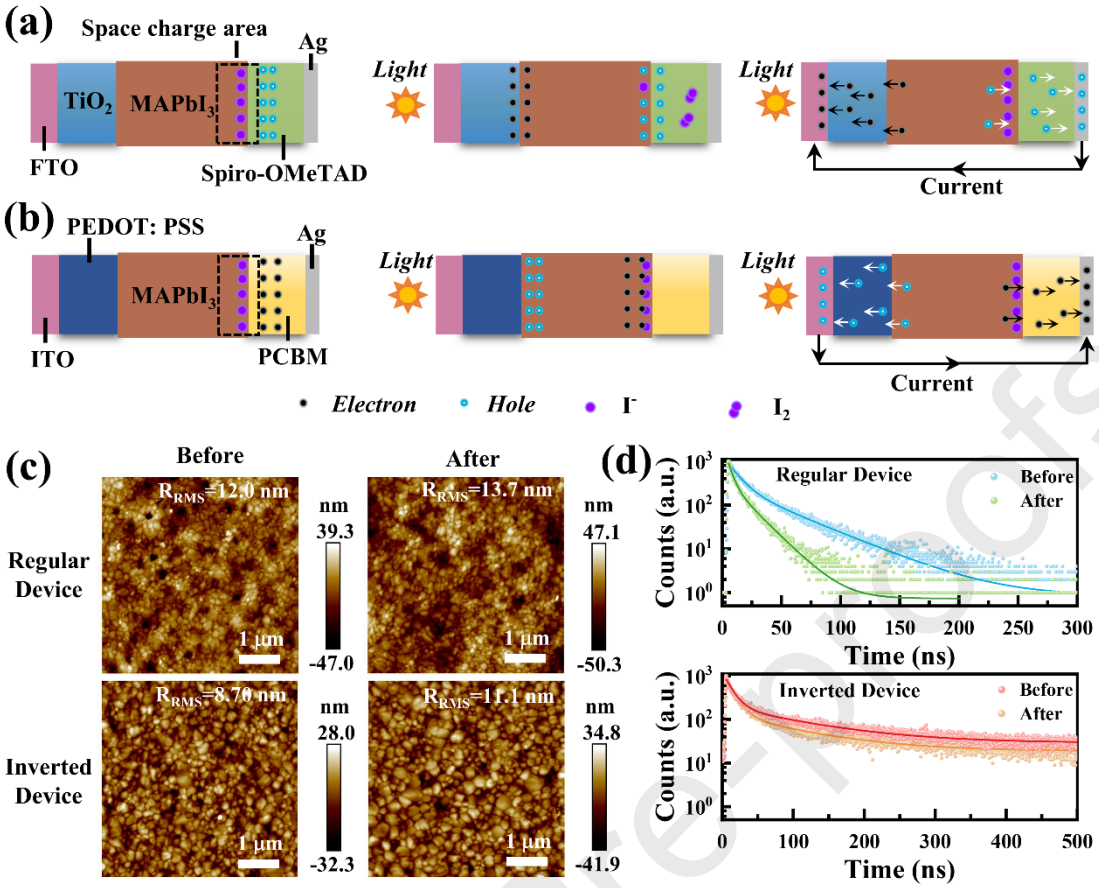

Figure 2. Mechanism of Ag stability variation in regular device (a), the device is stored in dark at open circuit with space charge region at $MAPbI_3$/spiro-OMeTAD interface, holes are captured by I^- to generate I_2 when device is illuminated at open circuit, carrier recombination takes place at external circuit when device is illuminated at short circuit. Mechanism of Ag stability variation in inverted device (b), the device is stored in dark at open circuit with space charge region at $MAPbI_3$/PCBM interface, photo-induced electrons gather at $MAPbI_3$/PCBM interface when device is illuminated at open circuit, carrier recombination takes place at external circuit when device is illuminated at short circuit. (c) AFM images obtained by the tapping mode, with the scale bar of 1 μm. The scanned dimension is 5 μm × 5 μm. (d) Time-resolved PL decay curves excited by a 375 nm laser.

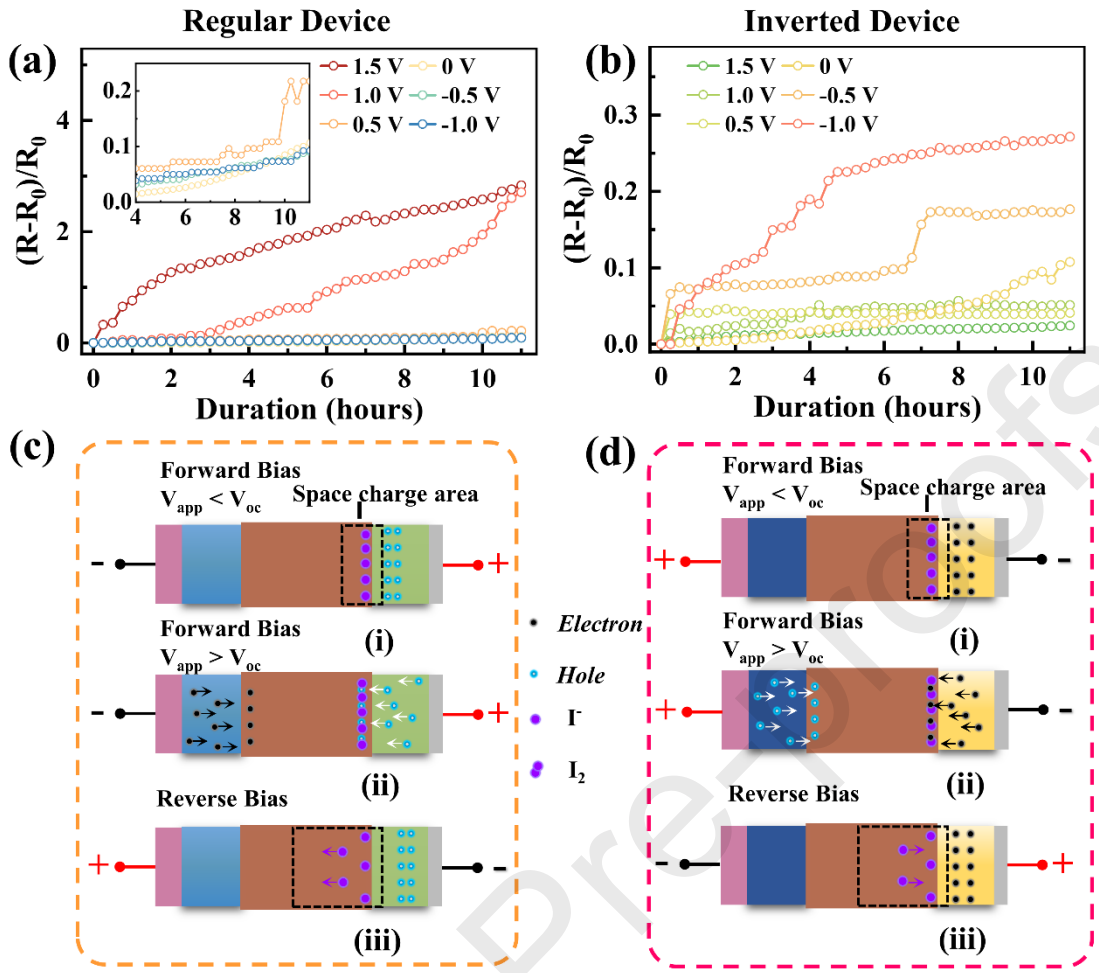

Figure 3. (a) The resistance variation of the Ag electrode on regular device under dark and bias condition. (b) The resistance variation of the Ag electrode on inverted device under dark and bias condition. (c) Mechanism of Ag stability variation in regular device, i. forward bias is applied to device and $V_{app} < V_{oc}$, ii. forward bias is applied to device and $V_{app} > V_{oc}$, iii. reverse bias is applied to device. (d) Mechanism of Ag stability variation in inverted device, i. forward bias is applied to device and $V_{app} < V_{oc}$, ii. forward bias is applied to device and $V_{app} > V_{oc}$, iii. reverse bias is applied to device.

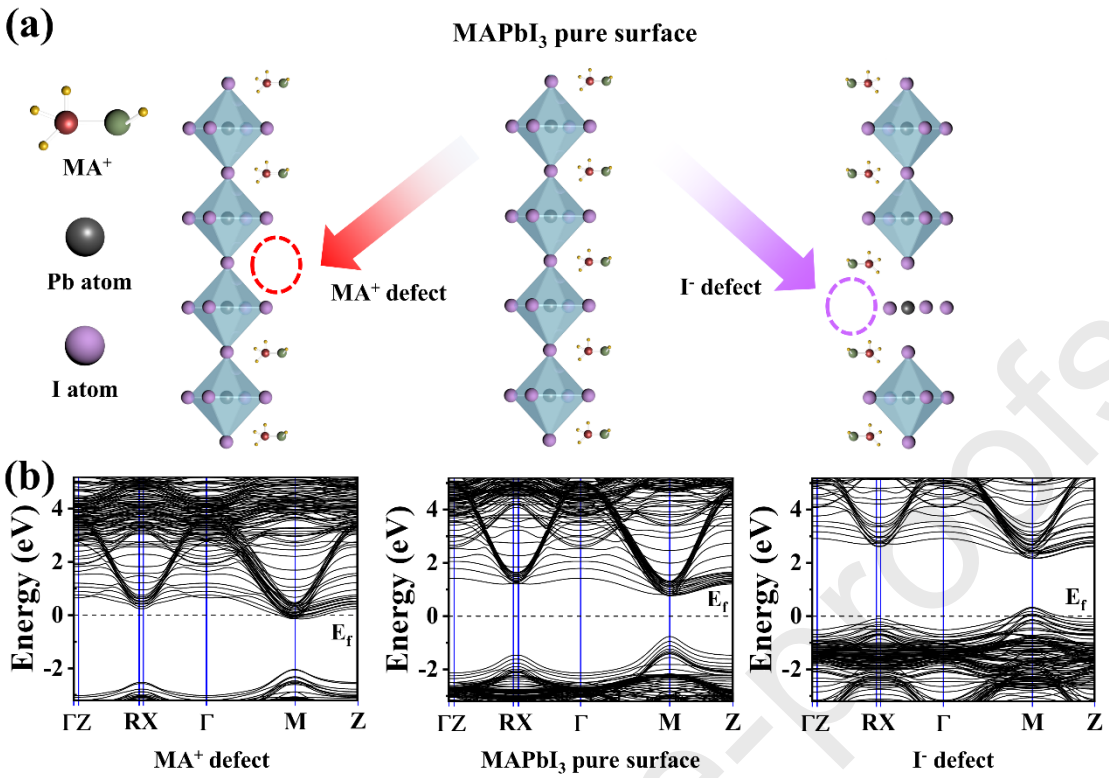

Figure 4. (a) Scheme of density functional theory (DFT) simulation model. (b) The band structure of different $MAPbI_3$ surface.

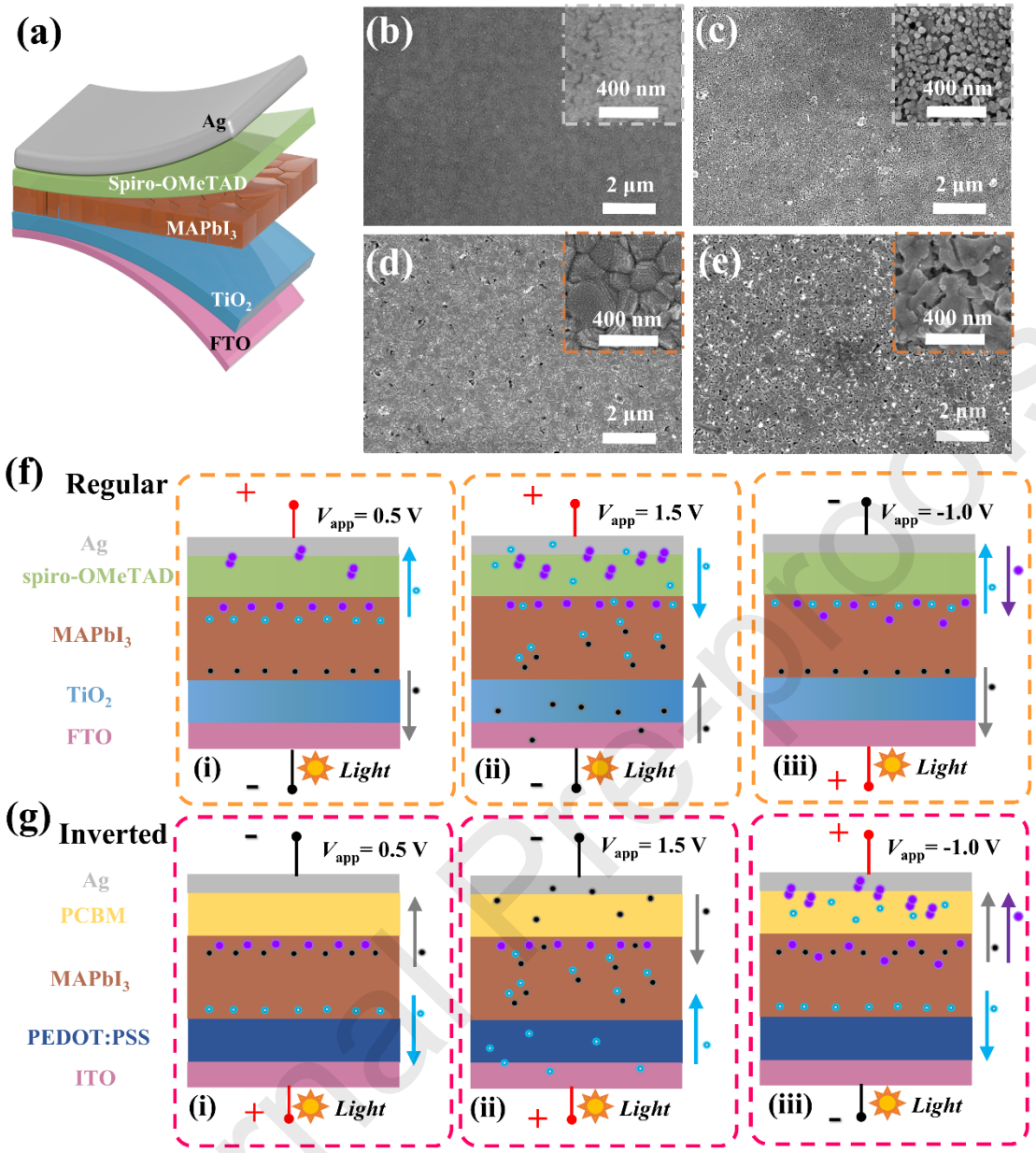

Figure 5. (a) The structure of regular device. SEM images at Ag electrode surface in regular device, (b) the new device, (c) the device after being tested under light and forward bias of 1.5V. SEM images at $MAPbI_3$ film surface in regular device after removal Ag/HTL, (d) the new device, (e) the device after being tested under light and forward bias of 1.5V. Mechanism of Ag stability variation under both light and bias, (f) in regular device: i. V_{app}=0.5 V, ii. V_{app}=1.5 V and iii. V_{app}=-1 V; (g) in inverted device: i. V_{app}=0.5 V, ii. V_{app}=1.5 V and iii. V_{app}=-1 V.

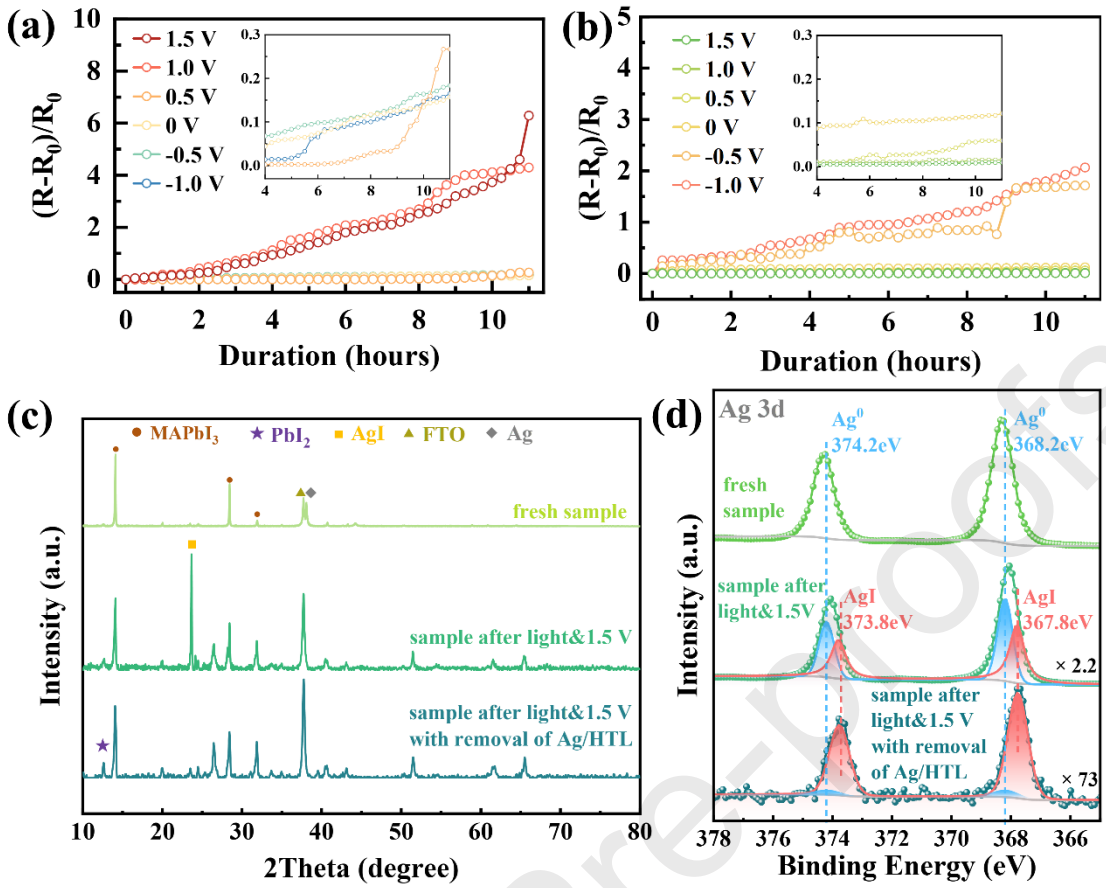

Figure 6. The resistance variation of the Ag electrode in devices with two structures under light and bias conditions, (a) regular structure, (b) reverse structure. (c) XRD results of different samples. (d) Binding energy peaks of Ag 3d of different samples.

TOC

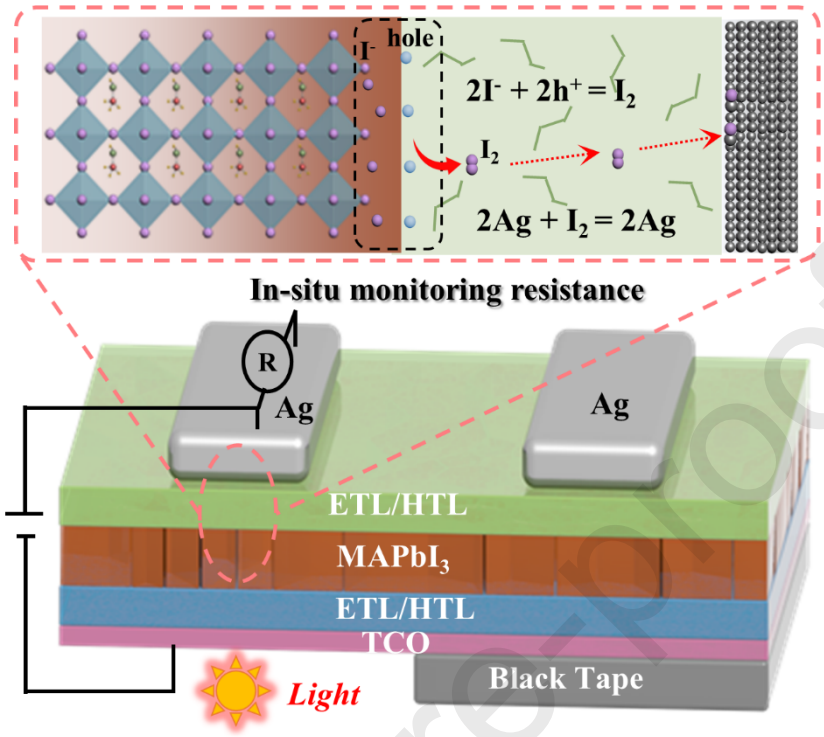

Highlights

- In-suit indicator of Ag electrode to inspect degradation of perovskite solar cells.
- Observation of stability evolution of two type devices under different conditions.
- Revealing the interaction process of accumulated charges and movable I^- defects.